Connection of scattering principles: a visual and mathematical tour

Filippo Broggini and Roel Snieder

Center for Wave Phenomena, Colorado School of Mines, Golden, CO 80401, USA

E-mail: fbroggin@mines.edu

Abstract
Inverse scattering, Green's function reconstruction, focusing, imaging and the
optical theorem are subjects usually studied as separate problems in different
research areas. We show a physical connection between the principles because
the equations that rule these *scattering principles* have a similar functional
form. We first lead the reader through a visual explanation of the relationship
between these principles and then present the mathematics that illustrates the
link between the governing equations of these principles. Throughout this work,
we describe the importance of the interaction between the causal and anti-causal
Green's functions.

1. Introduction

Inverse scattering, Green's function reconstruction, focusing, imaging and the optical
theorem are subjects usually studied in different research areas such as seismology [1],
quantum mechanics [2], optics [3], non-destructive evaluation of material [4] and medical
diagnostics [5].

    Inverse scattering [6–8] is the problem of determining the perturbation of a medium (e.g.
of a constant velocity medium) from the field scattered by this perturbation. In other words,
one aims to reconstruct the properties of the perturbation (represented by the scatterer in
figure 1) from a set of measured data. Inverse scattering takes into account the nonlinearity
of the inverse problem, but it also presents some drawbacks: it is improperly posed from the
point of view of numerical computations [9] and it requires data recorded at locations usually
not accessible due to practical limitations.

    Green's function reconstruction [10, 11] is a technique that allows one to reconstruct the
response between two receivers (represented by the two triangles at locations $\mathbf{R}_A$ and $\mathbf{R}_B$ in
figure 2) from the cross-correlation of the wavefield measured at these two receivers which are
excited by uncorrelated sources surrounding the studied system. In the seismic community,
this technique is also known as either the *virtual source method* [12] or *seismic interferometry*
[13, 14]. The first term refers to the fact that the new response is reconstructed as if one receiver
had recorded the response due to a *virtual* source located at the other receiver position; the
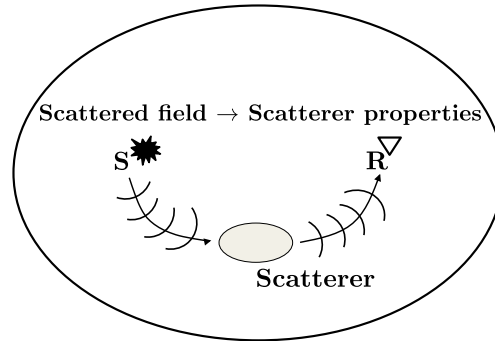
Figure 1. Inverse scattering is the problem of determining the perturbation of a medium from its scattered field.
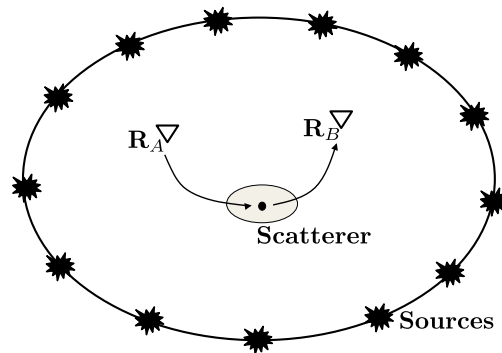

Figure 2. Green's function reconstruction allows one to reconstruct the response between two receivers (represented by the two triangles at locations $\mathbf{R}_A$ and $\mathbf{R}_B$).

second indicates that the recording between the two receivers is reconstructed through the 'interference' of all the wavefields recorded at the two receivers excited by the surrounding sources.

In this paper, the term *focusing* [15, 16] refers to the technique of finding an incident wave that collapses to a spatial delta function $\delta(x - x_0)$ at the location x_0 and at a prescribed time t_0 (i.e. the wavefield is focused at x_0 at t_0) as illustrated in figure 3. In a one-dimensional medium, we deal with a one-sided problem when observations from only one side of the perturbation are available (e.g. due to the practical consideration that we can only record reflected waves); otherwise, we call it a two-sided problem when we have access to both sides of the medium and account for both reflected and transmitted waves.

In seismology, the term *imaging* [17, 18] refers to techniques that aim to reconstruct an image of the subsurface (figure 4). Geologist and geophysicists use these images to study the structure of the interior of the Earth and to locate energy resources such as oil and gas. Migration methods [19, 20] are the most widely used imaging techniques and their accuracy depends on the knowledge of the velocity in the subsurface. Migration methods involve a single scattering assumption (i.e. the Born approximation) because these methods do not take
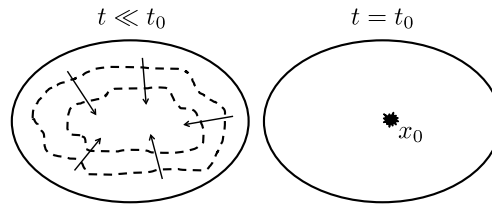
Figure 3. Focusing refers to the technique of finding an incident wavefield (represented by the dashed lines) that collapses to a spatial delta function $\delta(x-x_0)$ at the location x_0 and at a prescribed time t_0.
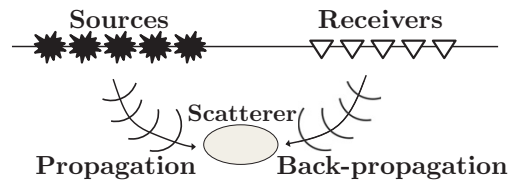

Figure 4. Imaging refers to techniques that aim to reconstruct an image of the subsurface.
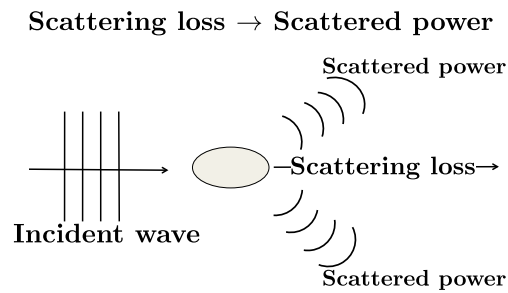

Figure 5. The optical theorem relates the power extinguished from a plane wave incident on a scatterer to the scattering amplitude in the forward direction of the incident field.

into account the multiple reflections that the waves experience during their propagation inside the Earth; hence, the data need to be preprocessed in a specific way before such methods can be applied.

The ordinary form of the *optical theorem* [2, 21] relates the power extinguished from a plane wave incident on a scatterer to the scattering amplitude in the forward direction of the incident field (figure 5). The scatterer casts a 'shadow' in the forward direction where the intensity of the beam is reduced and the forward amplitude is then reduced by the amount of energy carried by the scattered wave. The *generalized optical theorem* as originally formulated in [22] is an extension of the previous theorem and it deals with the scattering amplitude in all the directions; hence, it contains the ordinary form as a special case. This theorem relates the difference of two scattering amplitudes to an inner product of two other scattering amplitudes. The *generalized optical theorem* provides constraints on the scattering amplitudes in many scattering problems [23, 24]. Since these theorems are an expression of energy conservation,

Table 1. Principles and their governing equations in a simplified form. G is Green's function, f is the scattering amplitude and $*$ indicates complex conjugation.

	Principle	Equation
1	Inverse scattering	$u - u^* = \int u^* f$
2	Green's function reconstruction	$G - G^* = \int G G^*$
3	Optical theorem	$f - f^* = \int f f^*$
4	Imaging	$I = \int G G^*$

they are valid for any scattering system that does not involve attenuation (i.e. no dissipation of energy).

In this paper, we refer to the five subjects discussed above as *scattering principles* because they are all related, in different ways, to a *scattering* process. These principles are usually studied as independent problems but they are related in various ways; hence, understanding their connections offers insight into each of the principles and eventually may lead to new applications. This work is motivated by a simple idea: because the equations that rule these *scattering principles* have a similar functional form (see table 1), there should be a physical connection that could lead to a better comprehension of these principles and to possible applications.

To investigate these potential connections, we follow two different paths to provide maximum clarity and physical insights. We first show the relationship between different scattering principles using figures which lead the reader towards a visual understanding of the connections between the principles; then, we illustrate and derive the mathematics that shows the link between the governing equations of some of these principles.

2. Visual tour

In this section, we lead the reader through a visual understanding of the connections between different scattering principles.

2.1. Introduction of time–space diagrams

Before presenting the main results included in this section, we introduce and explain the time–space diagrams that appear in this paper. This particular visual representation is borrowed from the seismological community, where these time–space diagrams (called seismic sections) show the motion of the ground recorded by suitable receivers. Wavefields are represented as wiggle traces displaying travel time versus distance. We consider propagation and scattering of waves in a one-dimensional acoustic medium. The field equation governing the wave motion is $Lu(x, t) = 0$, where the acoustic wave equation differential operator is $L \equiv \rho(x) \frac{d}{dx} \left(\rho(x)^{-1} \frac{d}{dx} \right) - c(x)^{-2} \frac{d^2}{dt^2}$ [25], when the velocity and density of the medium are described by $c(x)$ and $\rho(x)$, respectively. To record the wavefield propagating inside the one-dimensional medium, we imagine to have receivers in the medium itself. As illustrated in figure 6(a), the white triangles correspond to receivers placed along the one-dimensional medium. We use a time–space finite difference code with absorbing boundary condition to simulate the propagation of the one-dimensional waves and to produce the numerical examples shown in this section.

We first consider a homogeneous medium with constant velocity $c(x)$ and density $\rho(x)$ shown in figures 6(c) and (d), respectively. We assume that a source injects energy at $x = 2$ km
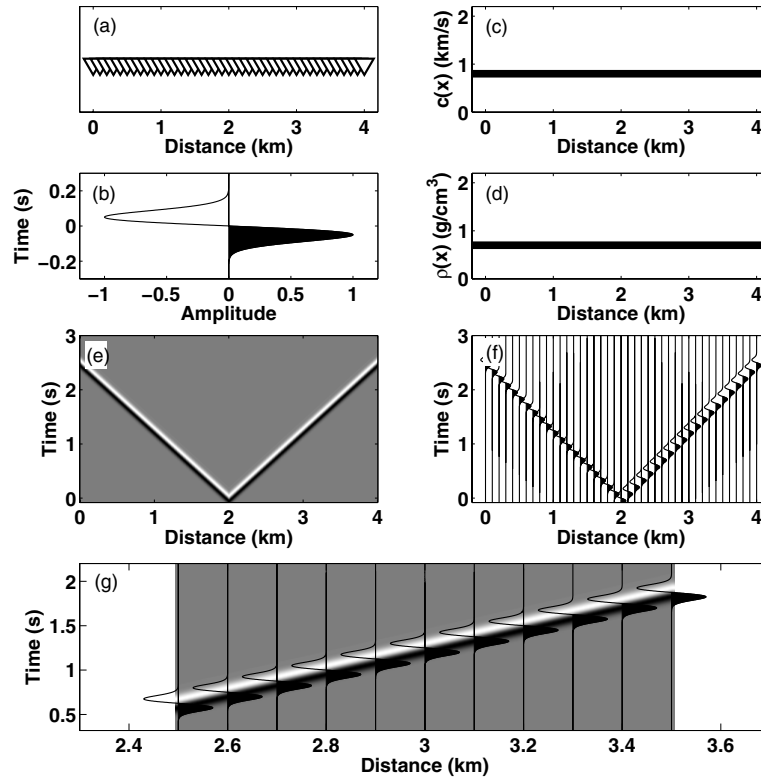
Figure 6. (a) The white triangles correspond to receivers in the one-dimensional medium with a spacing of 100 m. (b) Time dependence of the source function. (c) Velocity profile $c(x)$. (d) Density profile $\rho(x)$. (e), (f) Time–space diagrams for a source at $x = 2$ km. The traces are recorded by the receivers shown in (a). (g) Close-up of of the superposition of the time–space diagrams of (e) and (f).

with the source function described in figure 6(b) and measure the wavefield at every receiver. In this case, the wavefield is for $t > 0$ given by $u(x, t) = f(t - |x - x_s|/c) + f(t + |x - x_s|/c)$, where $f(t)$ is the source function shown in figure 6(b) and x_s is the source position. The wavefield $u(x, t)$ is shown in the time–space diagrams of figures 6(e) and (f). We show two different visualizations of $u(x, t)$ to facilitate the understanding of our wiggle representation. Figure 6(g) illustrates a closeup of a superposition of the two representations. Each vertical line (called trace) of figure 6(f) shows the wavefield measured by the receivers illustrated in figure 6(a). When the wavefield $u(x, t)$ assumes positive values, the area below $u(x, t)$ is filled to indicate such positive values in contrast to negative ones (as shown with the source function in figure 6(b)). The advantage of the wiggle traces over the contour plots is that one can better discern details of the waveforms. Causality ensures that the wavefield is nonzero only in the region $ct > |x - x_{\text{source}}|$ delimited by the first arrival (i.e. the direct waves). If we inject the source function of figure 7(a), we obtain the wavefield shown in figure 7(b). A similar diagram, for the same velocity and density profile, can be obtained for $t > 0$ if we simultaneously inject the same source at the locations $x = 0$ and $x = 4$ km, as shown in figure 7(c). Note that the two incident wavefields, emanating from $x = 0$ and $x = 4$ km, create a focus at $x = 2$ km at
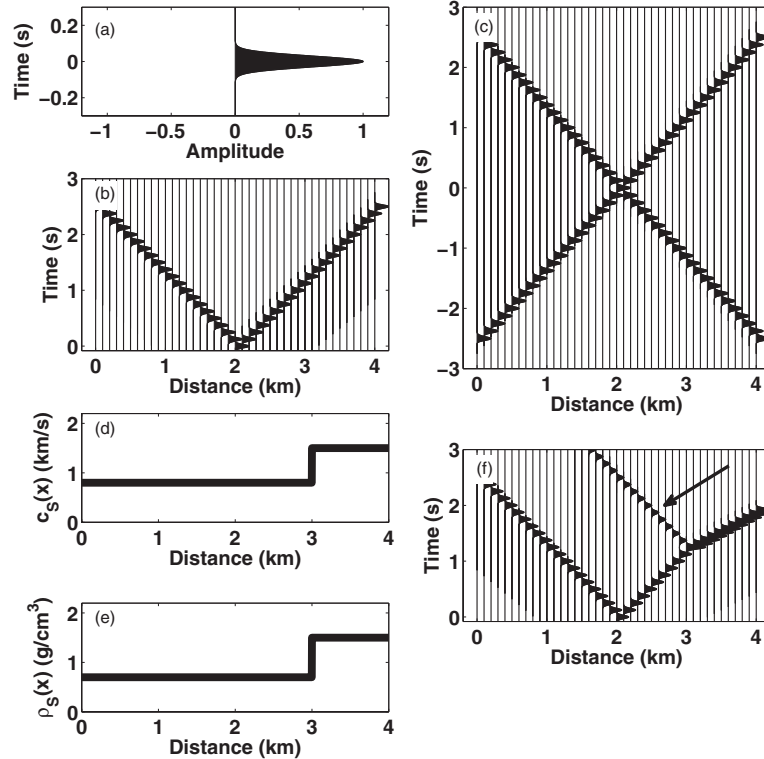
Figure 7. (a) Time dependence of the source signal. (b) Time–space diagram for a source at $x = 2$ km. The traces are recorded by the receivers shown in figure 6(a). (c) Time–space diagram when two sources are simultaneously present at $x = 0$ km and $x = 4$ km. (d) Velocity profile $c_s(x)$. (e) Density profile $\rho_s(x)$. (f) Time–space diagram when a source is present at $x = 2$ km in a medium described by $c_s(x)$ and $\rho_s(x)$. The traces are recorded by the receivers shown in figure 6(a). The arrow indicates the reflected waves.

$t = 0$ s. The time–space diagram of figure 7(c) is similar to the light cones described in special relativity [26].

This particular time–space diagram is easily created because the medium is homogeneous, but in a more complicated medium this is not trivial. We now consider another one-dimensional medium with velocity $c_s(x)$ and density $\rho_s(x)$ described in figures 7(d) and (e), respectively. In this case, the medium is not homogeneous; in fact, velocity and density are discontinuous. The incident wavefield emanates from $x = 2$ km, propagates towards the discontinuity in the model, interacts with it and generates transmitted and reflected scattered waves. The computed wavefield $u(x, t)$ is presented in the time–space diagram of figure 7(f) and the generation of the transmitted and reflected scattered waves is clearly visible at $x = 3$ km, corresponding to the step in the velocity and density profiles (figures 7(d) and (e)). The heterogeneity has two effects. First, there are now reflected waves within the 'light cone', as indicated by the arrow in figure 7(f). Second, the arrival time of the waves is crooked because of the changes in velocity.
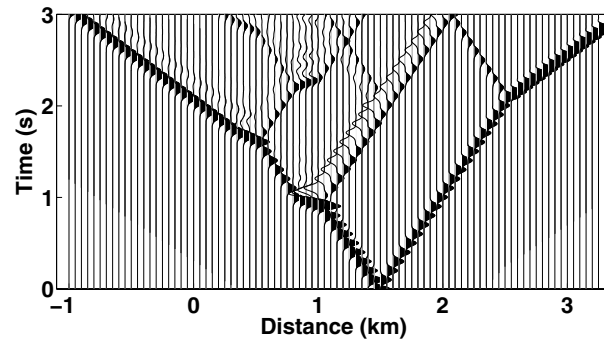
Figure 8. Scattering experiment with a source located at $x = 1.44$ km in the model shown in figure 9. The traces are recorded by receivers located in the model with a spacing of 40 m.

2.2. Main results

After this brief introduction regarding our visual notation, we can proceed to the core of this section. Figure 8 illustrates a scattering experiment in a more complicated one-dimensional acoustic medium where an impulsive source is placed at the position $x = 1.44$ km in the model shown in figure 9. The incident wavefield, a spatial delta function, propagates towards the discontinuities in the model, interacts with them and generates outgoing scattered waves. The computed wavefield is shown in the time–space diagram of figure 8 and it represents the causal Green's function of the system, G^+.

    Due to practical limitations, we usually are not able to place a source inside the medium we want to probe, which raises the following question: Is it possible to create the wavefield illustrated in figure 8 without having a real source at the position $x = 1.44$ km? An initial answer to such a question is given by Green's function reconstruction. This technique allows one to reconstruct the wavefield that propagates between a virtual source and other receivers located inside the medium [10]. We remind the reader that this technique yields a combination of the causal wavefield and its time-reversed version (i.e. anti-causal), because the reconstructed wavefield is propagating between a receiver and a *virtual source*. Without a real (physical) source, one must have non-zero incident waves to create waves that emanate from a receiver. In the next section, we introduce a mathematical argument to explain the interplay of the causal and anti-causal Green's functions. The fundamental steps to reconstruct Green's function are [13]

(1) measure the wavefields $G^+(x, x_{sl}, t)$ and $G^+(x, x_{sr}, t)$ at a receiver located at x (x varies from -1 km to 3 km) excited by impulsive sources located at both sides of the perturbation x_{sl} and x_{sr} (a total of two sources in 1D) as shown in figure 10;
(2) cross-correlate $G^+(x, x_{sl}, t)$ with $G^+(x_{vs}, x_{sl}, t)$, where $x_{vs} = 1.44$ km and vs stands for *virtual source*;
(3) cross-correlate $G^+(x, x_{sr}, t)$ with $G^+(x_{vs}, x_{sr}, t)$;
(4) sum the results computed at the two previous points to obtain $G^+(x, x_{vs}, t)$;
(5) repeat this for a receiver located at a different x.

The causal part of wavefield estimated by the Green's function reconstruction technique is shown in figure 11 and it is consistent with the result of the scattering experiment produced with a real source located at $x = 1.44$ km, shown in figure 8.
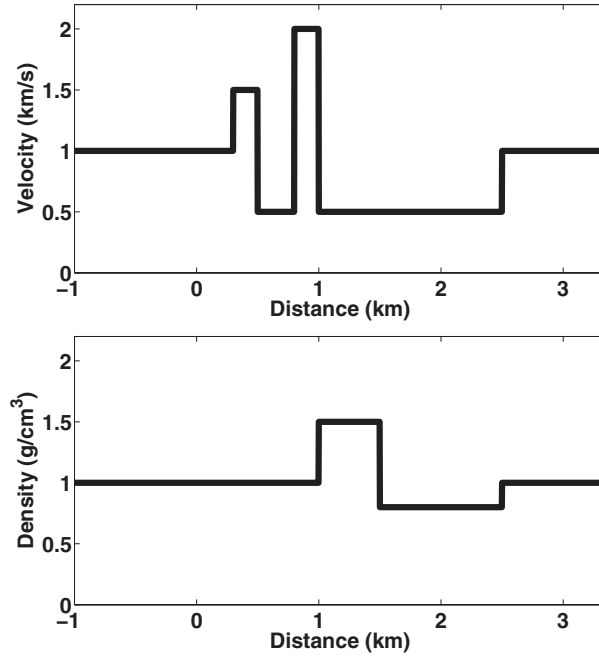
Figure 9. Velocity and density profiles of the one-dimensional model. The perturbation in the velocity is located between $x = 0.3$–2.5 km and $c_0 = 1$ km s^{-1}. The perturbation in the density is located between $x = 1.0$–2.5 km and $\rho_0 = 1$ g cm^{-3}.
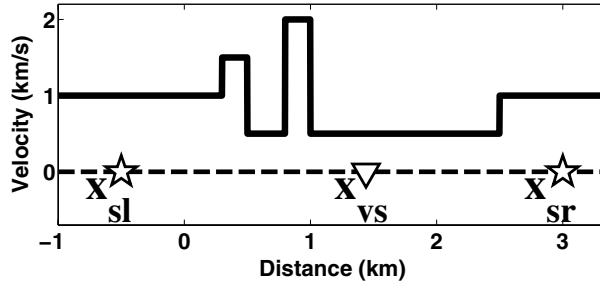

Figure 10. Diagram showing the locations of the real and virtual sources for seismic interferometry. x_{sl} and x_{sr} indicate the two real sources. x_{vs} shows the virtual source location.

We thus have two different ways to reconstruct the same wavefield, but often we are not able to access a certain portion of the medium we want to study and hence we cannot place any sources or receivers inside it. We next assume that we only have access to scattering data $R(t)$ measured on the left side of the perturbation, i.e. the reflected impulse response measured at $x = 0$ km due to an impulsive source placed at $x = 0$ km. This further limitation raises another question: Can we reconstruct the same wavefield shown in figure 8 having knowledge only of the scattering data $R(t)$? Since there are neither real sources nor receivers
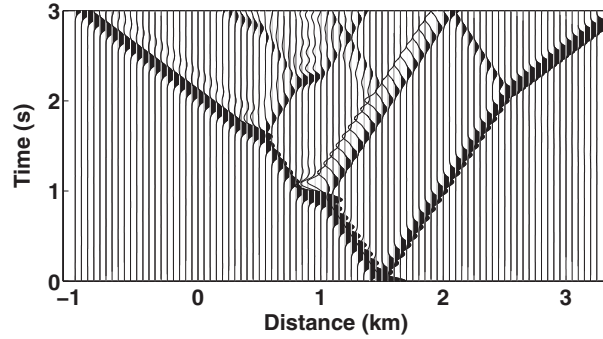
Figure 11. Causal part of the wavefield estimated by the Green's function reconstruction technique when the receiver located at $x = 1.44$ km acts as a virtual source.
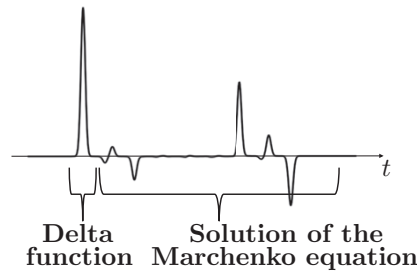

Delta   Solution of the
function Marchenko equation

Figure 12. Incident wave that focuses at location $x = 1.44$ km and time $t = 0$ s, built using the iterative process discussed by [15].

inside the perturbation, we speculate that the reconstructed wavefield consists of a causal and an anti-causal part, as shown in figure 14.

For this one-dimensional problem, the answer to this question is given in [15, 27]. The author of [15, 27] shows that we need a particular incident wave in order to collapse the wavefield to a spatial delta function at the desired location after it interacts with the medium, and that this incident wave consists of a spatial delta function followed by the solution of the Marchenko equation, as illustrated in figure 12.

The Marchenko integral equation [6, 28] is a fundamental relation of one-dimensional inverse scattering theory. It is an integral equation that relates the reflected scattering amplitude $R(t)$ to the incident wavefield $u(t, t_f)$ which will create a focus in the interior of the medium and ultimately gives the perturbation of the medium. The one-dimensional form of this equation is

$$0 = R(t + t_f) + u(t, t_f) + \int_{-\infty}^{t_f} R(t + t')u(t', t_f)\, dt', \tag{1}$$

where t_f is a parameter that controls the focusing location. We solve the Marchenko equation, using the iterative process described in detail in [27], and construct the particular incident wave that focuses at location $x = 1.44$ km, as shown in figure 8. After seven steps of the iterative process, we inject the incident wave in the model from the left at $x = -1$ km and compute the time–space diagram shown in the top panel of figure 13: it shows the evolution in time of the wavefield when the incident wave is the particular wave computed with the iterative
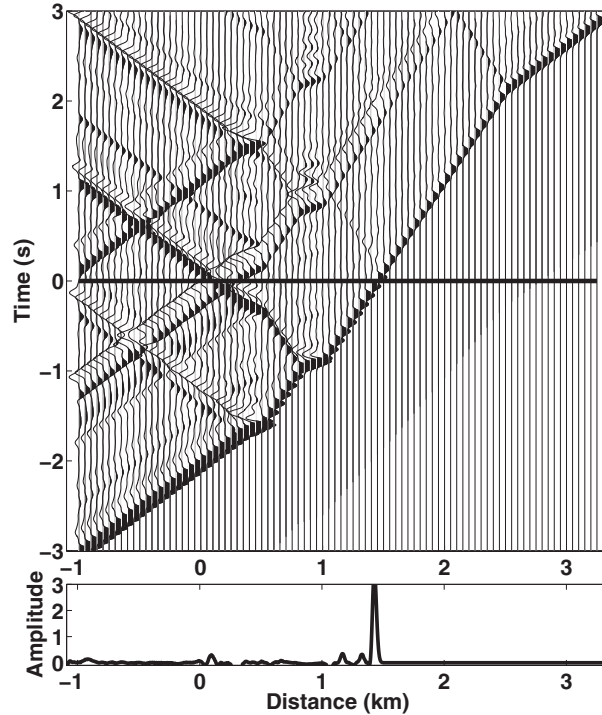
Figure 13. Top: after seven steps of the iterative process described in [27], we inject at $x = -1$ km the particular incident wave in the model and compute the time–space diagram. Bottom: cross-section of the wavefield at $t = 0$ s.

method. The bottom panel of figure 13 shows a cross-section of the wavefield at the focusing time $t = 0$ s: the wavefield vanishes everywhere except at location $x = 1.44$ km; hence, the wavefield focuses at this location. Note that the time derivative of the wavefield (i.e. the velocity) is not focused at $x = 1.44$ km; hence, the energy is also not focused at this location. We can thus create a focus at a location inside the perturbation without having a source or a receiver at such a location and without any knowledge of the medium properties; we only have access to the reflected impulse response measured on the left side of the perturbation. With an appropriate choice of sources and receivers, this experiment can be performed in practice (e.g. in a laboratory).

Figure 13 however does not resemble the wavefield shown in figures 8 and 11. But if we denote the wavefield in figure 13 as $w(x, t)$ and its time-reversed version as $w(x, -t)$, we obtain the wavefield shown in figure 14 by adding $w(x, t)$ and $w(x, -t)$. With this process, we effectively go from one-sided to two-sided illumination because in figure 14, waves are incident on the scatterer from both sides for $t < 0$ s. Reference [29] shows similar diagrams and explains how to combine such diagrams using causality and symmetry properties. The upper cone in figure 14 corresponds to the causal Green's function and the lower cone represents the anti-causal Green's function; the relationship between the two Green's functions is a key element in the next section, where we introduce the homogeneous Green's function G_h. Note
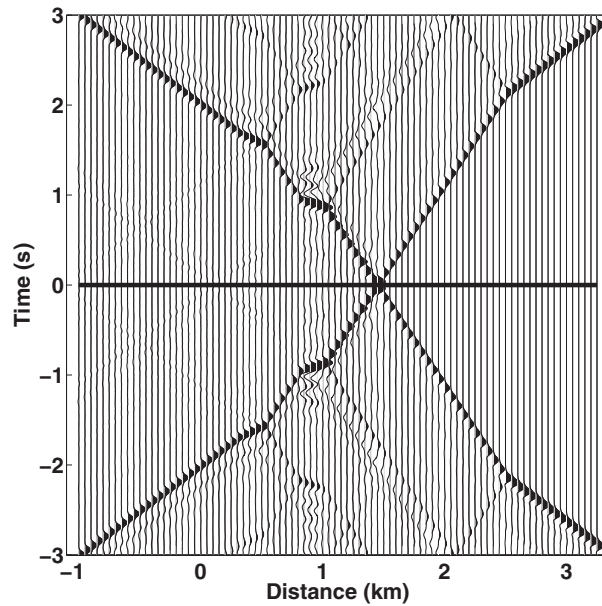
Figure 14. Wavefield that focuses at $x = 1.44$ km at $t = 0$ s without a source or a receiver at this location. This wavefield consists of a causal ($t > 0$) and an anti-causal ($t < 0$) part.
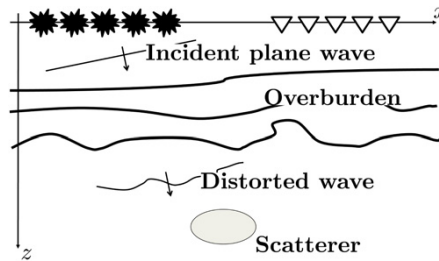

Figure 15. An incident plane wave created by an array of sources is injected in the subsurface. This plane wave is distorted due to the variations in the velocity inside the overburden (i.e. the portion of the subsurface that lies above the scatterer). When the wavefield arrives in the region that includes the scatterer, we do not know its shape.

that the wavefield in figure 14, with a focus in the interior of the medium, is based on reflected data recorded at the left side of the heterogeneity only. We did not use a source or receiver in the medium, and did not know the medium. All necessary information is encoded in the reflected waves. Note that a small amount of energy is present outside the two cones. This is due to numerical inaccuracies in our solution of the Marchenko equation.

The extension of the iterative process in two dimensions still needs to be investigated; but we conclude this section with a conjecture illustrated in figure 15. An incident plane wave created by an array of sources is injected in the subsurface where it is distorted due to the variations of the velocity inside the overburden (i.e. the portion of the subsurface that lies above the scatterer). Since we do not know the characteristics of the wavefield when it interacts
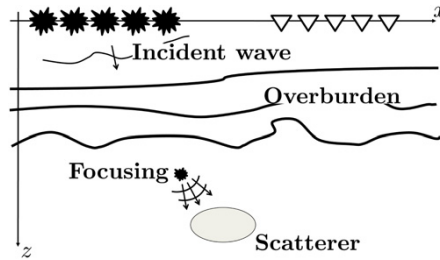
Figure 16. Focusing of the wavefield 'at depth'. A special incident wave, after interacting with the overburden, collapses to a point in the subsurface creating a buried source.
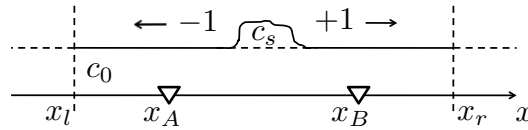

Figure 17. Geometry of the problem for the scattering of acoustic waves in a one-dimensional medium with constant density. x_A, x_B, x_l and x_r are the coordinates of the receivers (represented by the triangles) and the left and right bounds of our domain, respectively. The perturbation c_s is superposed on a constant velocity profile c_0.

with the region of the subsurface that includes the scatterer, it is difficult to reconstruct the properties of the scatterer without knowing the medium. Hence, following the insights gained with the one-dimensional problem, we would like to create a special incident wave that, after interacting with the overburden, collapses to a point in the subsurface creating a buried source, as illustrated in figure 16. In this case, assuming that the medium around the scatterer is homogeneous, we would know the shape of the wavefield that probes the scatterer and partially removes the effect of the overburden, which would facilitate accurate imaging of the scatterer.

3. Review of scattering theory

We review the theory for the scattering of acoustic waves in a one-dimensional medium (also called *line*) with a constant density (in contrast with the previous section where we also considered variable density), where the scatterer is represented by a perturbation of a constant velocity profile. Here, we introduce the wave equation and Green's functions that are used in the following section of the paper. Figure 17 shows the geometry of the scattering problem. The perturbation $c_s(x)$ is superposed on a constant velocity profile c_0. The following theory is developed in the frequency domain because it simplifies the derivations (e.g. convolution becomes a multiplication and derivatives become multiplications by $-i\omega$). We also show the time domain version of some of the following equations because they are more intuitive and allow us to understand the important role played by time reversal. The Fourier transform convention is defined by $\hat{f}(t) = \int f(\omega) \exp(-i\omega t)\, d\omega$ and $f(\omega) = (2\pi)^{-1} \int \hat{f}(t) \exp(i\omega t)\, dt$. Throughout this work, when we deal with a one-dimensional problem, the direction of propagation n assumes only two values, 1 and -1, which correspond to waves propagating to the right and to the left (figure 17), respectively.

The equation that governs the motion of the waves in an unperturbed medium with constant velocity c_0 is the constant-density acoustic homogeneous wave equation

$$L_0(x, \omega)u_0(n, x, \omega) = 0, \tag{2}$$

where u_0 is the displacement wavefield propagating in the n direction and the differential operator is

$$L_0(x, \omega) \equiv \left[\frac{\mathrm{d}^2}{\mathrm{d}x^2} + \frac{\omega^2}{c_0^2} \right]. \tag{3}$$

The solution of equation (2) is $u_0(n, x, \omega) = \exp(\mathrm{i}nx\omega/c_0)$ and its time-domain version is $\hat{u}_0(n, x, t) = \delta(t - nx/c_0)$, which is a delta function that propagates with velocity c_0 in the direction n representing a physical solution to the wave equation. The unperturbed Green's function satisfies the equation

$$L_0(x, \omega)G_0^{\pm}(x, x', \omega) = -\delta(x - x'), \tag{4}$$

and, in the acoustic one-dimensional case, its frequency-domain expression is [30]

$$G_0^{\pm}(x, x', \omega) \equiv \pm \frac{\mathrm{i}}{2k} \, \mathrm{e}^{\pm \mathrm{i}k|x-x'|}, \tag{5}$$

where $k \equiv \omega/c_0$. The $^+$ and $^-$ superscripts of Green's function represent the causal and anti-causal Green's function with outgoing or ingoing boundary conditions [31], respectively. In the time domain, causality implies that

$$\hat{G}_0^{\pm}(x, x', t) = 0 \qquad \pm t < |x - x'|/c_0. \tag{6}$$

Physically, the time-domain Green's function $\hat{G}_0^+(x, x', t)$ represents the displacement at a point x at time t due to a point source of unit amplitude applied at x' at time $t = 0$, while $\hat{G}_0^-(x, x', t)$ gives the displacement at x that is annihilated by a point source at x' at $t = 0$.

Next we consider the interaction of the wavefield u_0 with the perturbation $c_s(x)$ (see figure 17). This interaction produces a scattered wavefield $u_{sc}^{\pm}$; hence, the total wavefield can be represented as $u^{\pm} = u_0 + u_{sc}^{\pm}$. The $^+$ and $^-$ superscripts in the total wavefield indicate an initial and a final condition of the wavefield in the time domain, respectively:

$$\hat{u}^{\pm}(n, x, t) \rightarrow \hat{u}_0(n, x, t) \qquad t \rightarrow \mp\infty. \tag{7}$$

Physically, condition (7) with a plus sign means that the wavefield u^+, at early times, corresponds to the initial wavefield u_0 propagating forward in time in the n direction. The causal and anti-causal wavefields u^+ and u^- are related by time reversal; in fact, each one is the *time-reversed* version of the other $u^-(t) = u^+(-t)$. In the frequency domain, time reversal corresponds to complex conjugation: $u^-(\omega) = u^{+*}(\omega)$. Their *time reversal* relationship is better understood by comparing figures 18(a) and (b), which are valid for the velocity model of figure 9. Figure 18(b) is obtained by reversing the time axis of figure 18(a). We produced both figures using the same velocity model we used in section 2 of this paper (figure 9). In figure 18(a), the initial wavefield is a narrow Gaussian impulse injected at -1.5 km whereas in figure 18(b), the initial wavefield corresponds to the wavefield at $t = 6$ s in figure 18(a) and it coalesces to an outgoing Gaussian pulse.

The total wavefield $u^{\pm}$ satisfies the wave equation

$$L(x, \omega)u^{\pm}(n, x, \omega) = 0, \tag{8}$$

where the differential operator is

$$L(x, \omega) \equiv \left[\frac{\mathrm{d}^2}{\mathrm{d}x^2} + \frac{\omega^2}{c(x)^2} \right]. \tag{9}$$
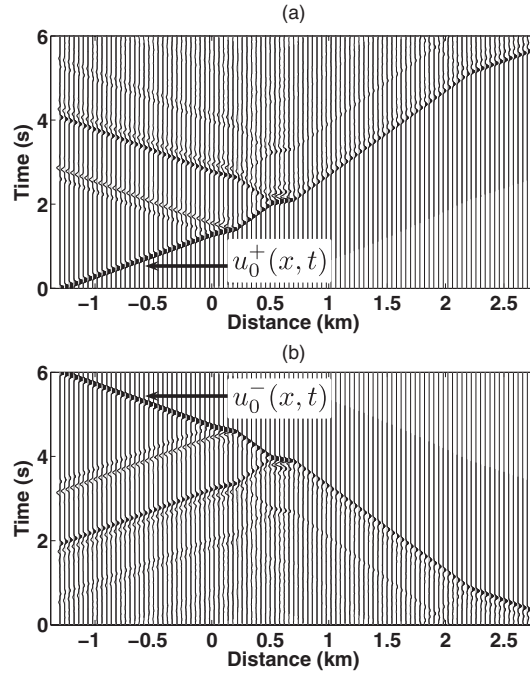
Figure 18. (a) The causal wavefield u^+ originated by a narrow Gaussian impulse injected at -1.5 km in the velocity model of figure 9. (b) The anticausal wavefield u^-. Note that each panel is the *time-reversed* version of the other.

The velocity varies with position, $c(x) = c_0 + c_s(x)$, as illustrated in figure 17. Using the operator L, we define the perturbed Green's function as the function that satisfies the equation

$$L(x, \omega)G^{\pm}(x, x', \omega) = -\delta(x - x'),$$ (10)

with the same boundary conditions as equation (5). Green's function $G^{\pm}$ takes into account all the interactions with the perturbation and hence it corresponds to the full wavefield propagating between the points x' and x, due to an impulsive source at x'.

4. Mathematical tour

In this part of the paper, we lead the reader through a mathematical tour and show that the different scattering principles have a common starting point, i.e. the following fundamental equation that reveals the connections between them:

$$G^+(x_A, x_B) - G^-(x_A, x_B)$$
$$= \sum_{x'=x_l, x_r} m\left[G^-(x', x_A)\frac{\mathrm{d}}{\mathrm{d}x}G^+(x, x_B)|_{x=x'} - G^+(x', x_B)\frac{\mathrm{d}}{\mathrm{d}x}G^-(x, x_A)|_{x=x'} \right]$$ (11)

with

$$m = \begin{cases} -1 & \text{if } x' = x_l \\ +1 & \text{if } x' = x_r, \end{cases}$$ (12)

where x_A, x_B, x_l and x_r (see figure 17) are the coordinates of the receivers located at x_A and x_B and the left and right bounds of our domain, respectively. Equation (11) (derived in appendix A) shows a relation between the causal and anti-causal Green's function and we refer to this expression, throughout the paper, as the representation theorem for the *homogeneous* Green's function $G_h \equiv G^+ - G^-$ [31], which satisfies the wave equation (10) when its source term is set equal to zero. G^+ and G^- both satisfy the same wave equation (10) because the differential operator L is invariant to time reversal ($LG^+ = -\delta$ and $LG^- = -\delta$); hence, their difference is source free: $L(G^+ - G^-) = 0$. The fact that $G^+ - G^-$ satisfies a homogeneous equation suggests that a combination of the causal and anti-causal Green's functions is needed to focus the wavefield at a location where there is no real source. This fact has been illustrated in the previous section when we reconstructed the same wavefield using the Green's function reconstruction technique and the inverse scattering theory (see figures 11 and 14); in both cases, we obtained a combination of the two Green's functions.

For the remainder of this paper, to be consistent with [32–34], we use the superscripts $^+$ and $^-$ to indicate the causal and anti-causal behaviour of wavefields and Green's functions, and, for brevity, we omit the dependence on the angular frequency ω.

4.1. Newton–Marchenko equation and generalized optical theorem

In this section, we show that equation (11) is the starting point to derive a Newton–Marchenko equation and a generalized optical theorem. In other words, we demonstrate how lines 1 and 3 of table 1 are linked to G_h. The Newton–Marchenko equation differs from the Marchenko equation because it requires both reflected and transmitted waves as data [35]. In contrast to the Marchenko equation (1), the Newton–Marchenko equation can be extended to two and three dimensions. The Marchenko and the Newton–Marchenko equations deal with the one-sided and two-sided problem, respectively. Following the work in [32–34], we manipulate equation (11) and show how to derive the equations that rule these two principles. Before starting with our derivation, we introduce some useful equations:

$$u^\pm(n, x) = u_0(n, x) + u_{sc}^\pm(n, x)$$
$$= u_0(n, x) + \int dx' G_0^\pm(x, x') L'(x') u^\pm(n, x'), \tag{13}$$

$$u^\pm(n, x) = u_0(n, x) + \int dx' G^\pm(x, x') L'(x') u_0(n, x'), \tag{14}$$

$$G^\pm(n, x, x') = G_0^\pm(n, x, x') + \int dx'' G^\pm(x, x'') L'(x'') G_0^\pm(n, x'', x'), \tag{15}$$

$$f(n, n') = -\int dx' e^{-nikx'} L'(x') u^+(n', x'), \tag{16}$$

where $L'(x) \equiv L(x) - L_0(x)$ describes the influence of the scatterer (perturbation). Equations (13), (14) and (15) are three different Lippmann–Schwinger equations [2]; they are a reformulation of the scattering problem using linear integral equations with a Green's function kernel. In particular, equation (13) shows that the total field is the summation of the incident wave $u_0(n, x)$ and the scattered wave $u_{sc}^\pm(n, x)$. The integral approach is also well suited for the study of inverse problems [8]. Equation (16) is the scattering amplitude [2] for an incident wave travelling in the n direction and that is scattered in the n' direction. We insert equation (15) into (11), simplify considering the fact that $x_r > x_A$, x'', x_B and $x_l < x_A$, x'', x_B,

and using expression (14)

$$G^+(x_A, x_B) - G^-(x_B, x_A) = \left(\frac{i}{2k}\right)\left(-\frac{i}{2k}\right)[iku^-(+1, x_A)u^+(-1, x_B)$$
$$+ iku^+(-1, x_B)u^-(+1, x_A) + iku^-(-1, x_A)u^+(+1, x_B)$$
$$+ iku^+(+1, x_B)u^-(-1, x_A)]. \tag{17}$$

In a more compact form, this can be written as

$$G^+(x_A, x_B) - G^-(x_B, x_A) = \left(\frac{i}{2k}\right)\sum_{n=-1,1} u^-(n, x_A)u^+(-n, x_B). \tag{18}$$

Equation (18) is the starting point to derive a Newton–Marchenko equation; we show the full derivation in appendix B and write the final result:

$$u^+(+1, x_A) - u^-(+1, x_A) = -\frac{i}{2k}\sum_{n=-1,1} u^-(n, x_A)f(n, x_B), \quad x_B > x_A, x'' \tag{19}$$

and

$$u^+(-1, x_A) - u^-(-1, x_A) = -\frac{i}{2k}\sum_{n=-1,1} u^-(n, x_A)f(n, -x_B), \quad x_B < x_A, x''. \tag{20}$$

The system of coupled equations (19) and (20) is our representation of the one-dimensional Newton–Marchenko equation [35]. Recognizing that $u^- = u^*$, equations (19) and (20) correspond to line 1 of table 1.

Next, following a similar derivation that led to equations (19) and (20), we insert expression

$$u^\pm(n, x) = u_0(n, x) + \int dx' G_0^\pm(x, x')L'(x')u^\pm(n, x') \tag{21}$$

into equation (19), we use the relation $u^-(n, x) = u^{+*}(-n, x)$ and equation (16), and we finally obtain a generalized optical theorem:

$$f(-n, n) + f^*(-n, n) = -\sum_{n'=-1,1} f(-n, n')f^*(n, n'), \tag{22}$$

where $f(n, n')$ represents the scattering amplitude [2] and n' assumes the value -1 or $+1$ (see line 3 of table 1). The obtained results are exact because in this one-dimensional framework we do not use any far-field approximations.

4.2. Green's function reconstruction and the optical theorem

Starting from the three-dimensional version of equation (11), reference [36] showed the connection between the generalized optical theorem and Green's function reconstruction. Following their three-dimensional formulation, we illustrate the same result for the one-dimensional problem and show the connection between lines 2 and 3 of table 1. In this part of the paper, we show the results and leave the mathematical derivation to appendix C. The expression for the one-dimensional Green's function reconstruction is

$$\frac{i}{2k}[G^+(x_A, x_B) - G^-(x_A, x_B)] = \sum_{x'=x_l, x_r} G^+(x_A, x')G^-(x_B, x'); \tag{23}$$

where Green's function excited by a point source at x_B recorded at x_A can be separated into an incident and a scattered part and is given by

$$G^\pm(x_A, x_B) = \underbrace{\mp\frac{i}{2k}\,e^{\pm ik|x_B - x_A|}}_{\text{direct}} \underbrace{\mp\frac{i}{2k}\,e^{\pm ik|x_B|}f(n, n')\,e^{ik|x_A|}}_{\text{scattered}}. \tag{24}$$
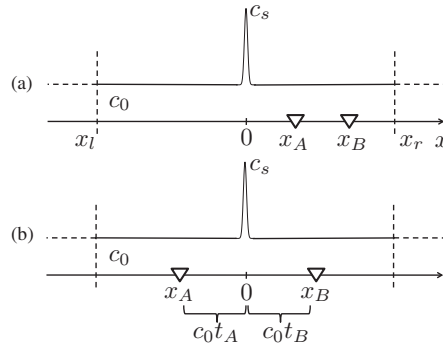
Figure 19. Configurations of the system used to show the connection between Green's function reconstruction and the optical theorem. In both cases, the receivers x_A and x_B are located outside the scatterer c_s, which is located at $x = 0$.

Unlike the three-dimensional case, we obtain two different results depending on the configuration of the system. In the first case (figure 19(a)), the ordinary optical theorem is derived:

$$f(n, n) + f^*(n, n) = -\sum_{n'=-1,1} |f(n, n')|^2; \tag{25}$$

in the second case (figure 19(b)), we obtain a generalized optical theorem

$$f(-n, n) + f^*(-n, n) = -\sum_{n'=-1,1} f(-n, n')f^*(n, n'), \tag{26}$$

where n assumes the value -1 or $+1$.

The above expressions of the optical theorem in one dimension agree with the work of the authors of [37] and differ from their three-dimensional counterpart because they contain the real part of the scattering amplitude instead of the imaginary part: $2\mathrm{Re} f(n, n) \equiv f(n, n) + f^*(n, n)$, where Re indicates the real part. We note that the ordinary form of the optical theorem (25) also follows from its generalized form (26) (the former is a special case of the latter). Furthermore, equation (26) is equivalent to the expression for the optical theorem derived in the previous section, equation (22). This is not surprising because both equations (26) and (22) have been derived from the same fundamental equation (11).

5. Conclusions

In section 2, we described the connection between different scattering principles, showing that there are three distinct ways to reconstruct the same wavefield. A physical source, the Green's function reconstruction technique, and inverse scattering theory allow one to create the same wavestate (see figure 8) originated by an impulsive source placed at a certain location x_s ($x = 1.44$ km in our examples). Green's function reconstruction show us how to build an estimate of the wavefield without knowing the medium properties, if we have a receiver at the same location x_s of the real source and sources surrounding the scattering region. Inverse scattering goes beyond this and allows us to focus the wavefield inside the medium (at location x_s) without knowing its properties, using only data recorded at one side of the medium. We showed that the interaction between causal and anti-causal wavefields is a key element to focus the wavefield where there is no real source; in fact, $G_h = G^+ - G^-$, which satisfies

the homogeneous wave equation (10), is a superposition of the causal and anti-causal Green's functions.

We speculate that many of the insights gained in our one-dimensional framework are still valid in higher dimensions. An extension of this work in two or three dimensions would give us the theoretical tools for many useful practical applications. For example, if we knew how to create the three-dimensional version of the incident wavefield shown in figure 12, we could focus the wavefield to a point in the subsurface to simulate a source at depth and to record data at the surface (figure 16); these kind of data are of extreme importance for full waveform inversion techniques [38] and imaging of complex structures (e.g. under salt bodies in seismic exploration [39]). Furthermore, we could possibly concentrate the energy of the wavefield inside a hydrocarbon reservoir to fracture the rocks and improve the production of oil and gas [40].

In the second part of this paper, the mathematical tour, we demonstrated that the representation theorem for the homogeneous Green's function G_h, equation (11), constitutes a theoretical framework for various scattering principles. We showed that all the principles and their equations (see table 1) rely on G_h as a starting point for their derivation. As mentioned above, the fundamental role played by the combination of the causal and anti-causal Green's functions has been evident throughout the mathematical tour: it is this combination that allows one to focus the wavefield to a location where neither a real source nor a receiver can be placed.

Acknowledgments

Appendix A. Derivation of equation (11)

Here, we derive equation (11), i.e. the representation theorem for the homogeneous Green's function. We start with the equations

$$\frac{d^2}{dx^2}G^+(x, x_B) + \frac{\omega^2}{c(x)^2}G^+(x, x_B) = -\delta(x - x_B) \tag{A.1}$$

and

$$\frac{d^2}{dx^2}G^-(x, x_A) + \frac{\omega^2}{c(x)^2}G^-(x, x_A) = -\delta(x - x_A), \tag{A.2}$$

where x_A, x_B and x indicate a position between x_l and x_r in figure 17. Next, we multiply equation (A.1) by $G^-(x, x_A)$, and equation (A.2) by $G^+(x, x_B)$; then, we subtract the two results and integrate between x_l and x_r, yielding

$$G^+(x_A, x_B) - G^-(x_B, x_A)$$
$$= \int_{x_l}^{x_r} dx \left[G^-(x, x_A) \frac{d^2}{dx^2}G^+(x, x_B) - G^+(x, x_B) \frac{d^2}{dx^2}G^-(x, x_A) \right]. \tag{A.3}$$

The right-hand side of the last equation is an exact derivative:

$$\int_{x_l}^{x_r} dx \left[G^-(x, x_A) \frac{d^2}{dx^2}G^+(x, x_B) - G^+(x, x_B) \frac{d^2}{dx^2}G^-(x, x_A) \right]$$
$$\equiv \int_{x_l}^{x_r} dx \frac{d}{dx} \left[G^-(x, x_A) \frac{d}{dx}G^+(x, x_B) - G^+(x, x_B) \frac{d}{dx}G^-(x, x_A) \right]; \tag{A.4}$$

hence, we obtain the expression for G_h:

$$G^+(x_A, x_B) - G^-(x_A, x_B)$$
$$= \sum_{x'=x_l, x_r} m\left[G^-(x', x_A)\frac{\mathrm{d}}{\mathrm{d}x}G^+(x, x_B)|_{x=x'} - G^+(x', x_B)\frac{\mathrm{d}}{\mathrm{d}x}G^-(x, x_A)|_{x=x'} \right] \quad \text{(A.5)}$$

with

$$m = \begin{cases} -1 & \text{if } x' = x_l \\ +1 & \text{if } x' = x_r, \end{cases} \quad \text{(A.6)}$$

where we have used the source–receiver reciprocity relation $G^\pm(x_A, x_B) = G^\pm(x_B, x_A)$ for the acoustic Green's function [41].

Appendix B. Derivation of the Newton–Marchenko equation

Inserting expression (15) into the left-hand side of equation (18), using the relation $u^+ = u_0 + u_{sc}^+$ on the right-hand side of (18), and then inserting (13) into the right-hand side, we get

$$\mathrm{e}^{+ik|x_A - x_B|} + \int \mathrm{d}x'' G^+(x_A, x'')L'(x'')\,\mathrm{e}^{+ik|x''-x_B|} + \mathrm{e}^{-ik|x_A - x_B|} + \int \mathrm{d}x'' G^-(x_A, x'')L'(x')\,\mathrm{e}^{-ik|x''-x_B|}$$
$$= u^-(+n, x_A)\,\mathrm{e}^{-ikx_B} + u^+(+n, x_A)\,\mathrm{e}^{+ikx_B}$$
$$+ \frac{i}{2k}u^-(+n, x_A)\int \mathrm{d}x''\,\mathrm{e}^{+ik|x_B - x''|}L'(x'')u^+(-n, x'')$$
$$+ \frac{i}{2k}u^-(-n, x_A)\int \mathrm{d}x''\,\mathrm{e}^{+ik|x_B - x''|}L'(x'')u^+(+n, x''). \quad \text{(B.1)}$$

In this one-dimensional problem, we need to consider two different cases: (1) $x_B > x_A, x''$ and (2) $x_B < x_A, x''$. Without loss of generality, we choose $x_B > x_A, x''$, and hence obtain

$$\mathrm{e}^{+ikx_B}\left[\mathrm{e}^{-ikx_A} + \int \mathrm{d}x'' G^+(x_A, x'')L'(x'')\,\mathrm{e}^{-ikx''}\right] + \mathrm{e}^{-ikx_B}\left[\mathrm{e}^{ikx_A} + \int \mathrm{d}x'' G^-(x_A, x'')L'(x'')\,\mathrm{e}^{+ikx''}\right]$$
$$= u^-(+1, x_A)\,\mathrm{e}^{-ikx_B} + u^-(-1, x_A)\,\mathrm{e}^{+ikx_B} - \frac{i}{2k}u^-(+1, x_A)\,\mathrm{e}^{+ikx_B}\int -\mathrm{d}x''\,\mathrm{e}^{-ikx''}L'(x')$$
$$\times u^+(-1, x'') - \frac{i}{2k}u^-(-1, x_A)\,\mathrm{e}^{+ikx_B}\int -\mathrm{d}x''\,\mathrm{e}^{-ikx''}L'(x'')u^+(+1, x''). \quad \text{(B.2)}$$

The terms inside the brackets on the left-hand side correspond to $u^+(-1, x_A)$ and $u^-(+1, x_A)$, respectively, whereas the integrals on the right-hand side correspond to $f(+1, -1)$ and $f(+1, +1)$, respectively. We rewrite equation (B.2) using (13), (14) and the relation $f(+n, +n') = f(-n', -n)$ to give

$$u^+(+1, x_A) - u^-(+1, x_A) = -\frac{i}{2k}\sum_{n=-1,1} u^-(n, x_A)f(n, x_B). \quad \text{(B.3)}$$

For the second case $x_B < x_A, x''$, the solution is

$$u^+(-1, x_A) - u^-(-1, x_A) = -\frac{i}{2k}\sum_{n=-1,1} u^-(n, x_A)f(n, -x_B). \quad \text{(B.4)}$$

Appendix C. Green's function reconstruction and the optical theorem

In this appendix, we derive the mathematics that shows the connection between the Green's function reconstruction equation and the optical theorem in one dimension. The expression for Green's function reconstruction is

$$\frac{i}{2k}[G^+(x_A, x_B) - G^-(x_A, x_B)] = \sum_{x'=x_l, x_r} G^+(x_A, x')G^-(x_B, x'), \tag{C.1}$$

and Green's function excited by a point source at x_s recorded at x_r is given by

$$G^+(x_r, x_s) = \underbrace{-\frac{i}{2k} e^{ik|x_s - x_r|}}_{Td} \underbrace{-\frac{i}{2k} e^{ik|x_s|} f(n, n') e^{ik|x_r|}}_{Ts}, \tag{C.2}$$

where $f(n, n')$ represents the scattering amplitude [2], and n' and n represent the directions of the incident wave and the scattered wave, respectively. In the expression above, Td represents the wave travelling directly from the source to the receiver, and Ts corresponds to the scattered wave that reaches the receiver after interacting with the scatterer. Considering the first configuration (figure 19(a)), inserting equation (C.2) into the right-hand side of equation (C.1), we get

$$\sum_{x'=x_l, x_r} G^+(x_A, x')G^-(x_B, x') = -\frac{i}{2k} \underbrace{\left[-\frac{i}{2k} e^{ik(x_B - x_A)} - \frac{i}{2k} e^{-ik(x_B + x_A)} f(-1, 1) \right]}_{T1}$$

$$-\frac{i}{2k} \underbrace{\left[-\frac{i}{2k} e^{-ik(x_B - x_A)} - \frac{i}{2k} e^{ik(x_B + x_A)} f^*(-1, 1) \right]}_{T2} - \left(\frac{i}{2k} \right)$$

$$\underbrace{\left(\frac{i}{2k} \right) e^{ik(x_B - x_A)} [f(-1, -1) + f^*(-1, -1) + |f(-1, -1)|^2 + |f(-1, 1)|^2]}_{T3}. \tag{C.3}$$

The terms $T1$ and $T2$ correspond to $G^+(x_A, x_B)$ and $-G^-(x_A, x_B)$, respectively, while the term $T3$ represents the unphysical wave previously discussed in the mathematical tour; hence, equation (C.3) simplifies to

$$\sum_{x'=x_l, x_r} G^+(x_A, x')G^-(x_B, x') = \frac{i}{2k}[G(x_A, x_B) - G^-(x_A, x_B)]$$

$$-\left(\frac{i}{2k} \right)^2 e^{ik(x_B - x_A)} [f(-1, -1) + f^*(-1, -1) + |f(-1, -1)|^2 + |f(-1, 1)|^2]. \tag{C.4}$$

For the right-hand side of equation (C.4) to be equal to the left-hand side of equation (C.1), the expression between the square brackets in term $T3$ should vanish:

$$f(-1, -1) + f^*(-1, -1) = -|f(-1, -1)|^2 + |f(-1, 1)|^2. \tag{C.5}$$

Equation (C.5) is the expression for the one-dimensional optical theorem [37]. The second configuration (figure 19(b)) gives

$$\sum_{x'=x_l, x_r} G^+(x_A, x')G^-(x_B, x') = \frac{i}{2k}[G^+(x_A, x_B) - G^-(x_A, x_B)] - \left(\frac{i}{2k} \right)^2 e^{ik(x_B + x_A)}$$

$$\times \underbrace{[f(-1, 1) + f^*(1, -1) + f(-1, -1)f^*(1, -1) + f(-1, 1)f^*(1, 1)]}_{T4}. \tag{C.6}$$

In this case, term $T4$ corresponds to the generalized optical theorem in one dimension [37].

The connection between Green's function reconstruction and the generalized optical theorem has not only a mathematical proof but also a physical meaning. The cross-correlation of scattered waves in equation (C.3) produces a *spurious* arrival [36], i.e. an unphysical wave that is not predicted by the theory. In the first configuration shown in figure 19(a), such *spurious* arrival has the same arrival time as the direct wave, $t_B + t_A$, but its amplitude is not correct (see term $T3$ in equation (C.3)). In the second case (figure 19(b)), t_A and t_B correspond to the time that a wave takes to travel from the origin $x = 0$ to x_A and x_B, respectively. Here, the *spurious* arrival corresponds to a wave that arrives at time $t_B - t_A$ when no physical wave arrives; in fact, it would arrive before the direct arrival at time $t_B + t_A$. But since the ordinary and generalized optical theorem hold, the *spurious* arrival cancels in both cases.

References

[1] Aki K and Richards P G 2002 *Quantitative Seismology* 2nd edn (Sausalito: University Science Books)
[2] Rodberg L S and Thaler R M 1967 *Introduction to the Quantum Theory of Scattering* (New York: Academic)
[3] Born M and Wolf E 1999 *Principles of Optics* (Cambridge: Cambridge University Press)
[4] Shull P J 2002 *Nondestructive Evaluation: Theory, Techniques, and Applications* (Boca Raton, FL: CRC Press)
[5] Epstein C L 2003 *Mathematics of Medical Imaging* (Upper Saddle River, NJ: Prentice-Hall)
[6] Chadan K and Sabatier P C 1989 *Inverse Problems in Quantum Scattering Theory* 2nd edn (Berlin: Springer)
[7] Gladwell G M L 1993 *Inverse Problems in Scattering* (Alphen aan den Rijn: Kluwer)
[8] Colton D and Kress R 1998 *Inverse Acoustic and Electromagnetic Scattering Theory* (Berlin: Springer)
[9] Dorren H J S, Muyzert E J and Snieder R 1994 *Inverse Problems* **10** 865–80
[10] Wapenaar K, Fokkema J and Snieder R 2005 *J. Acoust. Soc. Am.* **118** 2783–6
[11] Larose E, Margerin L, Derode A, van Tiggelen B, Campillo M, Shapiro N, Paul A, Stehly L and Tanter M 2006 *Geophysics* **71** SI11–SI21
[12] Bakulin A and Calvert R 2006 *Geophysics* **71** SI139–SI150
[13] Curtis A, Gerstoft P, Sato H, Snieder R and Wapenaar K 2006 *Leading Edge* **25** 1082–92
[14] Schuster G T 2009 *Seismic Interferometry* (Cambridge: Cambridge University Press)
[15] Rose J H 2001 *Phys. Rev.* A **65** 012707
[16] Rose J H 2002 *Time Reversal, Focusing and Exact Inverse Scattering (Imaging of Complex Media with Acoustic and Seismic Waves)* ed M Fink, W A Kuperman, J P Montagner and A Tourin (Berlin: Springer)
[17] Claerbout J F 1985 *Imaging the Earth's Interior* (Oxford: Blackwell)
[18] Sava P and Hill S J 2009 *Leading Edge* **28** 170–83
[19] Bleistein N, Cohen J and Stockwell J 2001 *Mathematics of Multidimensional Seismic Imaging, Migration, and Inversion* (Berlin: Springer)
[20] Biondi B 2006 *3D Seismic Imaging* (Tulsa, OK: Society of Exploration Geophysicists)
[21] Newton R G 1976 *Am. J. Phys.* **44** 639–42
[22] Heisenberg W 1943 *Z. Phys.* **120** 673–02
[23] Marston P 2001 *J. Acoust. Soc. Am.* **109** 1291
[24] Carney P, Schotland J and Wolf E 2004 *Phys. Rev.* E **70** 036611
[25] Fokkema J T and van den Berg P M 1993 *Seismic Applications of Acoustic Reciprocity* (Amsterdam: Elsevier)
[26] Ohanian H C and Ruffini R 1994 *Gravitation and Spacetime* 2nd edn (New York: Norton)
[27] Rose J H 2002 *Inverse Problems* **18** 1923–34
[28] Lamb G L 1980 *Elements of Soliton Theory* (New York: Wiley)
[29] Burridge R 1980 *Wave Motion* **2** 305–23
[30] Snieder R 2004 *A Guided Tour of Mathematical Methods for the Physical Sciences* 2nd edn (Cambridge: Cambridge University Press)
[31] Oristaglio M 1989 *Inverse Problems* **5** 1097–105
[32] Budreck D E and Rose J H 1990 *Inverse Problems* **6** 331–48
[33] Budreck D E and Rose J H 1991 *SIAM J. Appl. Math.* **51** 1568–84
[34] Budreck D E and Rose J H 1992 *J. Math. Phys.* **33** 2903–15
[35] Newton R G 1980 *J. Math. Phys.* **21** 493–505
[36] Snieder R, van Wijk K, Haney M and Calvert R 2008 *Phys. Rev.* E **78** 036606
[37] Hovakimian L 2005 *Phys. Rev.* A **72** 064701
[38] Brenders A J and Pratt R G 2007 *Geophys. J. Int.* **168** 133–51
[39] Sava P and Biondi B 2004 *Geophys. Prospect.* **52** 607–23
[40] Beresnev I A and Johnson P A 1994 *Geophysics* **59** 1000–17
[41] Wapenaar K and Fokkema J 2006 *Geophysics* **71** SI33–SI46